Evolution of the Local Spiral Structure Revealed by OB-type Stars in Gaia DR3

Q. A. Ge[1,2], J. J. Li[1], C. J. Hao[1], Z. H. Lin[1], L. G. Hou[3], D. J. Liu[1], Y. J. Li[1], and S. B. Bian[1]
[1] Purple Mountain Observatory, Chinese Academy of Sciences, Nanjing 210023, People's Republic of China; jjli@pmo.ac.cn
[2] School of Astronomy and Space Science, University of Science and Technology of China, Hefei 230026, People's Republic of China
[3] National Astronomical Observatories, Chinese Academy of Sciences, 20A Datun Road, Chaoyang District, Beijing 100101, People's Republic of China

Accepted for AJ

Reporter:Lin Zhang（张琳）

Mar 28, 2025

Outline

- Introduction
- Sample
- Result
- Summary

Introduction

- The structure, as well as the formation and evolution of galactic spiral arms, is one of the fundamental problems in astronomy. The evolution of spiral structure can be studied by examining the differences in spiral patterns traced by objects of different ages, which also provides observational constraints on the formation mechanisms of a galaxy’s spiral arms (e.g., Dobbs & Baba 2014).
- Some studies have found observational evidence of offsets between the arms traced by old and young objects (e.g., Martínez-García et al. 2009; Martínez-García & González-Lópezlira 2011;Yu&Ho2018), while others do not (e.g., Seigar et al. 2006; Foyle et al. 2011; Davis et al. 2012).
- However, directly studying the offsets between the Galactic spiral arms traced by objects of different ages has long been a challenge, primarily due to the lack of appropriate methods that can yield accurate distances for a large number of old stars.

Introduction

- Before Gaia, possible offsets between different components were mainly studied using the tangency directions of the Galactic spiral arms (e.g., Hammersley et al. 1999; Drimmel & Spergel 2001; Churchwell et al. 2009; Vallée 2014a, 2014b; Hou & Han 2015; Vallée 2016).
- Fortunately, the abundant data obtained with the high-precision astrometric satellite Gaia have provided precise distance measurements (e.g., Maíz Apellániz et al. 2021) for a vast number of stars, including many OB stars (e.g., Maíz Apellániz et al. 2020, 2022) and evolved stars in the vicinity of the Sun (Gaia Collaboration et al. 2016, 2018, 2021, 2023a).
- Recently, research on mapping the Galactic spiral structure based on the three-dimensional positions of evolved stars (R.A., decl., and parallax) is gradually achieving success(e.g., Poggio et al. 2018 , 2021, Lin et al. 2022).

Introduction

- Although previous studies have traced the spiral arms in the solar neighborhood using evolved stars (e.g., turn-off, red clump, and UMS stars), these studies were either limited to a small area in the Galactic disk (e.g., Miyachi et al. 2019; Lin et al. 2022) or contained a mix of objects of various ages.
- Therefore, to reveal better the possible evolutionary properties of nearby spiral arms, a large sample of stars with age determinations and accurate distances is crucial.
- We aim to use the OB stars of different ages to understand the possible offsets and evolution processes of the spiral arms in the solar neighborhood.

Sample

Selecting OB stars from Gaia DR3

- effective temperature : 10,000 < *teff_esphs* < 50,000 K
- distance from the Galactic plane : d < 300 pc
- astrometric fidelity indicator: f_a > 0.5 (Rybizki et al. 2022)
- tangential velocity: v_{tan} < 180 $km\ s^{-1}$ (Gaia Collaboration et al. 2023b)
- selected only stars with a parallax precision better than 20%, i.e., *parallax_over_error* > 5
- removed sources fainter than the main-sequence stars (e.g., white dwarfs and subdwarfs) , $(\pi/100)^5 < 10^{(2-G+1.8*(G_{BP}-G_{RP}))}$ (where π represents the parallax of the star; Gaia Collaboration et al. 2023c)
- the RR-Lyrae stars identified by *vari_rryrae* in Gaia DR3 were removed

A total of 383,987 OB stars were obtained.

Sample

- In order to understand the spiral structure traced by stars with different ages, we referenced the correspondence between effective temperature and spectral type for OB stars (Pecaut & Mamajek 2013) and divided the sample into five groups, corresponding to O–B2, B3–B5, B6–B7, B8, and B9 stars, respectively.

Table 1
Number of Stars in Each Group and Their Approximate Effective Temperature ($T_{\rm eff}$) Ranges and Average Age

Group Members	Number	$T_{\rm eff}$ (K)[(1)]	Average Age (Myr)[(2,3,4,5)]
O–B2	28,802	>20,000	12
B3–B5	46,251	15,700–20,000	35
B6–B7	40,824	14,000–15,700	60
B8	75,787	12,300–14,000	110
B9	212,507	10,000–12,300	160

References. (1) Pecaut & Mamajek (2013; Version: 2022 April 16), (2) Chen et al. (2013), (3) Daszyńska-Daszkiewicz & Miszuda (2019), (4) Levenhagen & Leister (2004), and (5) Liu et al. (2023).

- Due to the lack of astrophysical parameters for the brighter stars, there is a decreased apparent density of stars selected based on their effective temperature within about 1 kpc of the Sun (Gaia Collaboration et al. 2023c).

- To address this issue, the OB stars in the catalog of Skiff (2014) are adopted. This catalog contains 68,612 OB stars collected from the literature and was last updated on 2020 February 6.

Sample

We performed a crossmatch between these OB stars and the Gaia DR3 catalog with a matching radius of 1″ and eliminated targets with more than one positionally matched Gaia source.

Based on the selection criteria of $parallax\_over\_error > 5$ and $f_a > 0.5$, and after removing redundant sources, we obtained 20,184 spectroscopically confirmed OB stars.

Then we assigned these 20,184 stars to the various groups according to their spectral type given by the Skiff catalog.

The parallaxes and effective temperatures of 404,171 OB stars are listed in Table 2.

Table 2
Sample of OB Stars Used in This Work

Gaia DR3 ID (1)	R.A. (deg) (2)	Decl. (deg) (3)	π (mas) (4)	$T_{\rm eff}$ (K) (5)	Spectral Type (6)
1195551392247930	43.8815	2.0182	6.701 ± 0.059	10,940	B9
3793113252920320	45.6663	5.1881	4.938 ± 0.038	10,541	B9
7352369831088510	46.4401	6.5208	3.316 ± 0.038	10,181	B9
7957921564970750	43.1653	6.4747	4.210 ± 0.048	11,275	B9

Note. Column (1) lists the Gaia DR3 ID of each source; columns (2) and (3) show the R.A. and decl. values, respectively; column (4) gives the parallaxes and their errors; column (5) provides the effective temperatures ($T_{\rm eff}$); and column (6) gives the spectral types based on $T_{\rm eff}$ (Pecaut & Mamajek 2013) or from the Skiff catalog (Skiff 2014).

(This table is available in its entirety in machine-readable form in the online article.)

Result --- 3.1. Nearby Spiral Structure Traced by O–B2 Stars

To highlight the differences in the density distributions of stars on the spiral arms and the interarm regions, we show the distributions of stellar overdensity, Δ_Σ, (Poggio et al. 2021, Lin et al. 2022) which is a relative dimensionless quantity and defined as:

$$\Delta_\Sigma(X, Y) = \frac{\Sigma(X, Y) - \langle\Sigma(X, Y)\rangle}{\langle\Sigma(X, Y)\rangle}.$$

Here, the local surface density $\Sigma(X, Y)$ and the mean surface density $\langle\Sigma(X, Y)\rangle$ are estimated using Epanechnikov kernel density estimators with bandwidths of 0.3 and 2 kpc (e.g., Lin et al. 2022), respectively.

This method has the advantage of reducing the influence of the exponential distribution of disk stars on the map and making the spiral arms more evident compared to a map obtained by directly using the surface density distributions.

Result

Triangles: High-mass stellar formation regions (HMSFR) masers

We overlaid the HMSFR masers from Reid et al. (2019) on the overdensity map of O–B2 stars, which reveals good agreement in the arm positions.

Therefore, we used these O–B2 stars to indicate the nearby spiral arms defined by young objects, which are then compared with the spiral structure traced by older objects to understand the possible evolution of the Galactic spiral arms.

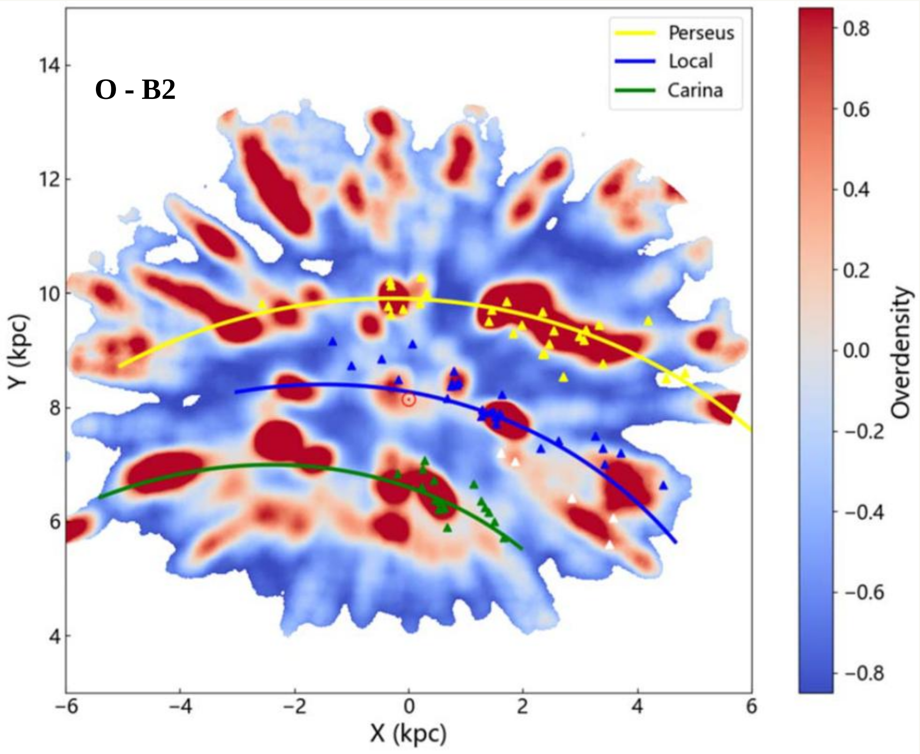

Figure 1. Overdensity map of O–B2 stars. The solid curved lines of different colors indicate the centers of the fitted spiral arms given by Xu et al. (2023): the Perseus Arm (yellow), the Local Arm (blue), and the Carina Arm (green). The white filled triangles indicate masers located in the spur between the Local Arm and the Carina Arm (Xu et al. 2016). The position of the Sun is shown by a red Sun symbol at (X, Y) = (0, 8.15) kpc (Reid et al. 2019), and the Galactic center is at (X, Y) = (0, 0) kpc.

Result --- 3.2. Evolution of the Spiral Arms in the Solar Neighborhood

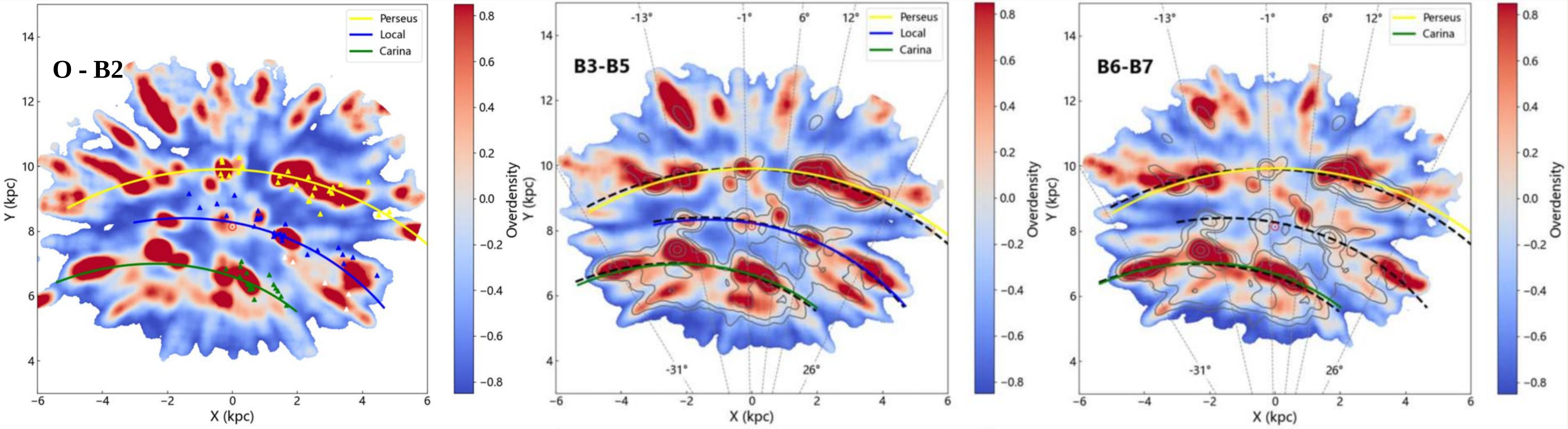

solid curved lines: the centers of the fitted spiral arms given by Xu et al. (2023)

solid curved lines: the centers of the fitted spiral arms in this work; black dashed lines: the centers of the fitted spiral arms given by Xu et al. (2023); gray dashed lines: the Galactocentric azimuthal angle β.

The overdensity distribution of B3–B5 stars presents three major spiral arms in the solar vicinity, and the fitted spiral arms are generally in agreement with that traced by the O–B2 stars.

There are significant differences in the distributions near the Local Arm defined by the O–B2 stars in the third and fourth Galactic quadrants, where no obvious overdensities of B6–B7 stars appear.

Result

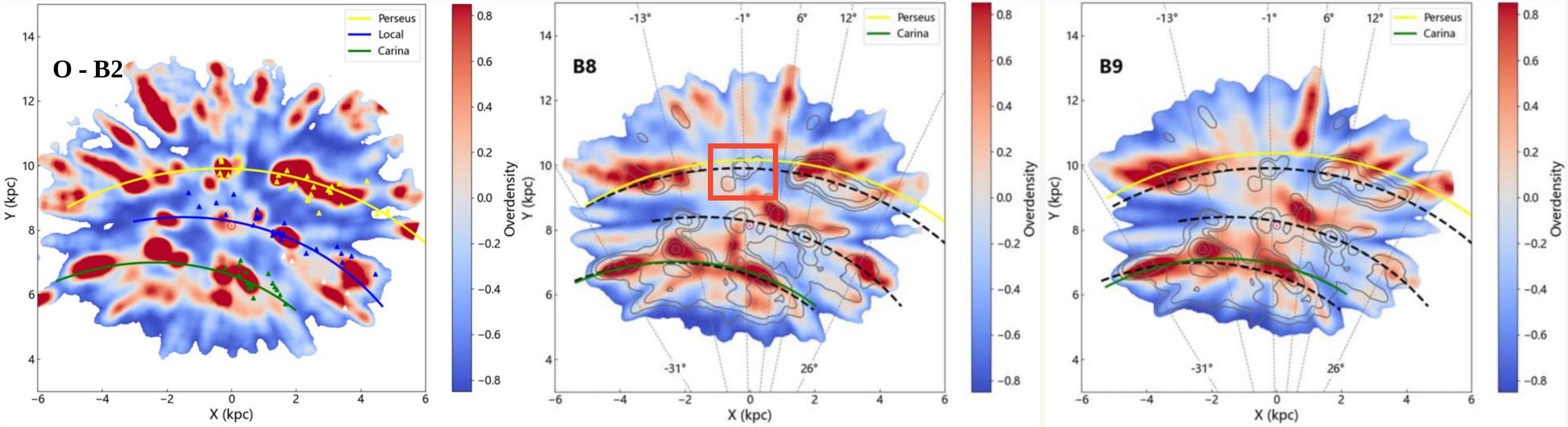

In the directions of β ranging from -5° to 2°, the overdensity of B8 stars near the Perseus Arm almost disappears, resulting in the appearance of a discontinuity in the Perseus Arm across the second and third Galactic quadrants.

The B8 stars near the Perseus Arm are further away from the Galactic center, which appear to have a collective shift toward the anti-Galactic center direction, especially in the second Galactic quadrant.

The offsets of the spiral arms fitted by the B9 stars are even more pronounced.

Result --- 3.3. Offsets of Nearby Spiral Arms at Different Azimuth Angles

The scatterplot in each panel highlights the changes in the overdensity peaks for the Carina Arm and the Perseus Arm.

B3–B5 stars: When comparing the results of the B3–B5 and O–B2 stars in different β directions, both groups exhibit significant overdensities near the spiral arms, with offsets corresponding to the peaks not exceeding 0.11 kpc.

B6–B7 stars: Larger offsets appear in the directions of β = −31° and −1°, and the corresponding offsets of the Carina Arm are 0.13 and 0.15 kpc.

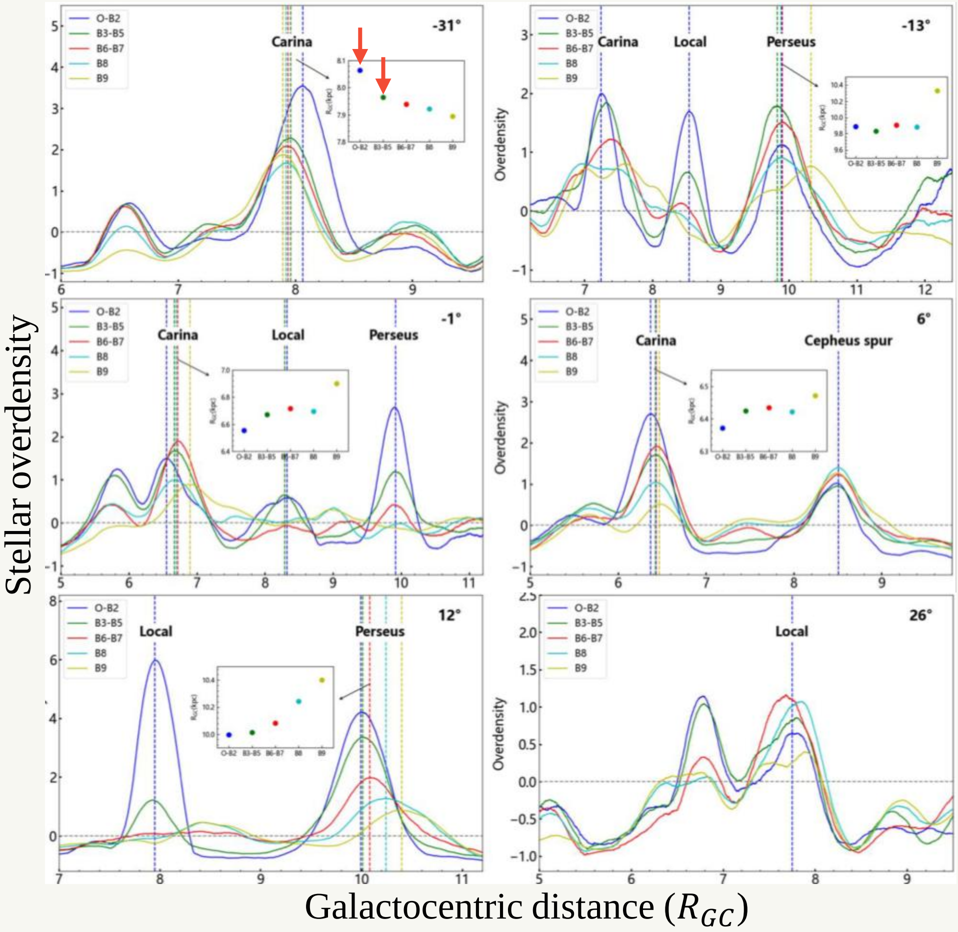

Result --- 3.3. Offsets of Nearby Spiral Arms at Different Azimuth Angles

B8 stars: In the directions of β = −31° and β = −1°, the overdensity peak of the Carina Arm is offset by 0.14 kpc relative to that of the O–B2 stars. At β = 12°, the offset of the Perseus Arm increases to 0.25 kpc.

B9 stars: In the directions of β = −13° and β = 12°, the offsets of the overdensity peaks in the Perseus Arm are 0.44 and 0.34 kpc, respectively. In the direction of β = −31°, the offset of the overdensity peak of the Carina Arm is 0.32 kpc.

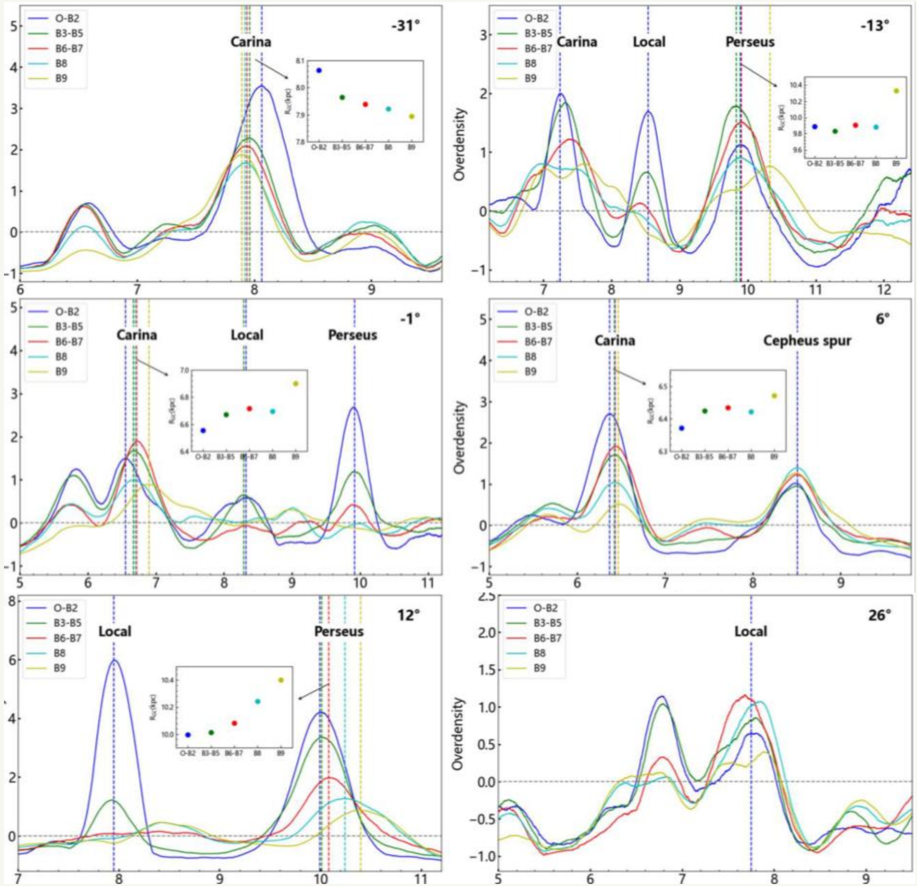

Stellar overdensity

Galactocentric distance (R_{GC})

Summary

- We have used 404,171 OB stars younger than 200 Myr from Gaia DR3, and categorized them into different age groups (OB2, B3–B5, B6–B7, B8, and B9 stars), to investigate the evolution of the local spiral arm structure.

- Similar to the spiral arms traced by OCs, which gradually blur with increasing age (Hao et al. 2021), the overall overdensities of spiral arms show a weakening trend with increasing age of the OB tracer stars.

- As the ages of the OB stars increase, the Perseus Arm traced by them gradually shifts toward the anti-Galactic center direction, which supports the conclusion that offsets exist in the gaseous and (old) stellar components of the different spiral arms, which were found through an analysis of the tangential arm directions (Hou & Han 2015), and the pitch angle of the Carina Arm gradually decreases.

- For the Local Arm, as the ages of the OB tracer stars increase, in the region of approximately $\beta < 0^\circ$, the overdensity near the Local Arm gradually disappears.

Thank you!